Tellus (2002), 54A, 529–541
Printed in UK. All rights reserved

TELLUS
ISSN 0280–6495

Simulating the Greenland atmospheric boundary layer

Part II: Energy balance and climate sensitivity

By BRUCE DENBY*, WOUTER GREUELL and JOHANNES OERLEMANS, *Institute for Marine and Atmospheric Research, Utrecht University, Princetonplein 5, 3584 CC Utrecht, The Netherlands*

(Manuscript received 7 December 2001; in final form 22 April 2002)

ABSTRACT

A three-dimensional dynamic downscaling model of the Greenland atmospheric boundary layer is used to investigate the surface energy balance of the Greenland ice sheet for the summer ablation season of 1998. The model is forced by ECMWF analysis data and has a horizontal resolution of 20 km. The results show that the turbulent heat fluxes contribute significantly (32%) to the total surface energy flux in the ablation region. A climate sensitivity experiment is carried out with the model by increasing the free atmospheric forcing temperature by 1 K. The resulting change, known as climate sensitivity, in 2 m temperature, 2 m wind speed and the surface energy balance components are discussed. The 2 m temperature is shown to have a climate sensitivity significantly less than unity, as low as 0.3, in regions where melt prevails for most of the ablation season. The surface energy flux in the ablation region is found to increase by 21% for a 1 K increase in atmospheric temperature. Wind speeds also increase, particularly near the margin of the ice sheet, as a result of enhanced katabatic forcing. Enhanced wind speeds are shown to account for roughly 12% of the climate sensitivity of the sensible heat flux when averaged over the ablation region. Albedo feedback is also shown to play an important role in the total climate sensitivity of the surface energy balance.

1. Introduction

The ablation component of the surface mass balance for the Greenland ice sheet is dependent on the surface energy flux at the surface. When surface temperatures reach the melting point the excess energy can be used to melt the ice or snow surface. Some of this melt will refreeze in the snow pack, but a large portion will be lost through drainage. The surface energy balance (SEB) that determines the net surface energy flux consists of the four components of short- and longwave radiation, and sensible and latent turbulent heat fluxes. In general the absorption of shortwave radiation is the most important term in this energy balance; however, the other terms are also significant. In fact, changes in atmospheric temperature are transmitted to the surface chiefly via these three other components. As such it is important to understand their contribution to the SEB.

When one is modelling the mass balance of the Greenland ice sheet the surface ablation must be determined. This can be done using degree day models, which are based on empirical relationships that link integrated temperatures directly to melt using a degree day factor, or by determining the SEB, which is based on the physical processes that occur at the surface. If physically based processes are to be included, then use of the SEB is the preffered choice for calculating melt rates. In mass balance models, such as those employed by van de Wal (1996) and Zuo and Oerlemans (1996) which are driven by SEB calculations, simplified forms of the SEB are used. In particular, the turbulent heat fluxes are parameterised as a linear expression of near surface temperature, which itself is based on a climatological parameterisation, e.g. Ohmura (1987).

*Corresponding author.
e-mail: bd236@cam.ac.uk
Present address: Scott Polar Research Institute, University of Cambridge, Lensfield Road, Cambridge, CB2 1ER, UK.

An alternative to prescribing the turbulent heat fluxes in this fashion is to run large-scale meteorological models, such as GCMs and weather prediction models, that calculate directly the SEB and the accumulation rates. These models are in general marred by a lack of resolution. The ablation zone of the Greenland ice sheet is, at its widest extent, no greater than 100 km, and on average around 30 km, so it would require model resolutions of this order or less to attempt to model the surface ablation. Thompson and Pollard (1997) and Glover (1999) have used GCMs with a horizontal resolution of 2.5° (300 km) to simulate precipitation and melt on the Greenland ice sheet. This is clearly too coarse a resolution to be used on the ablation zone and they have, through necessity, downscaled their results using assumed lapse rates and wind fields. Results from these studies indicate an overestimation of ablation by a factor of 2–6 when compared to observational estimates (Warwick et al., 1996). A GCM simulation by Ohmura et al. (1996) used a model resolution of 1° (125 km), which gave improved estimates of ablation without downscaling in spite of its inability actually to resolve the ablation zone. ECMWF analysis data are currently available, with a resolution of approximately 63 km. Even so, this still does not resolve the ablation zone properly, and some form of downscaling is clearly needed to calculate the SEB in order to resolve the ablation zone.

In a concurrent paper (Denby et al., 2002), referred to as DEN1, the Greenland atmospheric boundary layer model (GABLM) is used to simulate the atmospheric boundary layer (ABL) over Greenland at a horizontal resolution of 20 km. This model is a dynamic downscaling model that takes 'off line' free atmospheric meteorological fields from an already existing model, in this case ECMWF analysis data, and forces the Greenland ABL with them. In this way improved resolution can be obtained and the physical processes of the ABL can be properly incorporated.

In DEN1 the model is described and compared to observations made on the ice sheet by six automatic weather stations (AWS) during the 1998 ablation season. The results from DEN1 show quite good agreement between the simulated and observed variables of wind, temperature and specific humidity and improve significantly on the results taken directly from ECMWF analysis data. Simulated temperatures tend to be slightly too high at all sites, with a mean difference of 0.6 °C when averaged over the summer period, and average wind speeds are within 0.7 m s^{-1} of their observed values, with the exception of one site near the ice margin where simulated wind speeds were systematically lower, -1.5 m s^{-1}, than those observed. At this site the 20 km model resolution underestimates surface slope and hence katabatic forcing. A comparison of the simulated SEB with observed melt also shows good agreement for one of the sites (S5) but overestimates the surface ablation by 35% at another site (S6).

In DEN1 the SEB is calculated for the six AWS involved in the comparison. In this second study, the model simulation is used to calculate the SEB of the entire Greenland ice sheet during the same summer ablation season and to determine the climate sensitivity of the model to a change in free atmospheric temperature. In this paper the climate sensitivity of any parameter is defined as being its sensitivity to a change in free atmospheric temperature. The climate sensitivity of 2 m temperature, wind and the surface energy fluxes to a change in atmospheric temperature is investigated in order to identify the relative importance of the various energy flux components. In particular, the climate sensitivity of the turbulent heat fluxes is analysed as well as the climate sensitivity of the katabatically forced winds.

2. Model description

The model used for this study is described in detail in DEN1 but the main points will be summarised here. As stated in that paper, the GABLM uses meteorological fields from an already existing model, in this case ECMWF analysis data, and forces the ABL model with these fields. The prescribed fields used are:

1. Geopotential height at 700 hPa to determine geostrophic winds. These are assumed to be barotropic and thus constant with height.
2. Free atmospheric temperature specified as a linear function of height taken by fitting ECMWF data from above the ABL up to a height of approximately 4 km.
3. Relative humidity field taken from ECMWF data at a height of approximately 1200 m above the surface.
4. Cloud cover from ECMWF total cloud cover analysis. Low, medium or high cloud covers are not distinguished and cloud height is set at approximately 3500 m above the surface.

5. Monthly mean sea surface temperatures from ECMWF analysis.

With the exception of sea surface temperatures, these fields are updated every 12 h, 00 and 12 GMT, and linearly interpolated in time. The specific humidity field is prescribed only at the lateral and top boundaries of the model whilst the free atmospheric temperature field and synoptic pressure gradient field is prescribed directly in the model field itself by splitting them into synoptic, taken directly from ECMWF analysis, and perturbation fields.

Attenuation of the incoming shortwave radiation by atmosphere and clouds is parameterised using schemes from van de Wal (1994) and Konzelmann et al. (1994), whilst an emissivity scheme from Garratt and Brost (1982) is used to calculate the longwave radiation. Subsurface temperatures are initialised on the basis of the 2 m temperature parameterisation from Ohmura (1987), and the subsurface temperature is calculated using a temperature diffusion model. Surface roughness lengths and subsurface parameters are also specified on the basis of the temperature parameterisation from Ohmura (1987). Albedo is determined internally using a two-layer snow model which calculates albedo as a function of melt and snow depth. These parameterisation schemes and initialisations are described in detail in DEN1.

The Greenland model topography and land/ice/sea mask is taken from the EKHOLM 0.02° data set (Ekholm, 1996). All ice regions, including those not directly associated with the ice sheet, are included in the calculations.

The ABL simulation is carried out using a 20 km horizontal grid resolution. 20 vertical layers, up to a maximum height of 5 km, are used with a lowest level height of 2 m. The number of vertical levels in the subsurface temperature diffusion model is 15 and the lowest level is placed at 10 m below the surface, with an upper level depth of 5 mm.

The model is run using ECMWF input fields taken from the 1998 ECMWF analysis data starting on 20 May 1998, day 140, and ending on 28 August 1998, day 240. A 10 d spin up time is allowed and mean values for the 90 d summer period, from day 150 to day 240, are derived. This simulation is known as the reference run and is equivalent to the simulation described in DEN1. A climate sensitivity run is also made where the free atmospheric temperature is increased by 1 K over the entire model domain.

3. Surface energy balance

The surface energy balance (SEB) can be written as:

$$\mathrm{GFL} = \mathrm{NSW} + \mathrm{NLW} + \mathrm{HFL} + \mathrm{EFL} \quad (1)$$

where GFL is the total surface energy flux, NSW is the net shortwave radiation flux, NLW is the net longwave radiation flux, HFL is the turbulent sensible heat flux and EFL is the turbulent latent heat flux. These are defined as positive downwards and expressions for these fluxes can be found in DEN1.

The SEB from the 1998 GABLM simulation is presented in this section for the entire Greenland ice sheet. The four SEB components and the total surface energy flux averaged over the summer period are shown for all points on the ice sheet in Fig. 1. The SEB is presented as a function of the surface extrapolated free atmospheric temperature T_a. This parameter is used since it is an independent forcing parameter of the model, taken from the ECMWF analysis data. The mean value of T_a over the summer period can be well approximated by the following parameterisation, indicating its dependence on height above sea level (a.s.l.), h, and latitude, ϕ:

$$T_a(\phi, h) = 8.8 - 0.0052h - 0.11(\phi - 72). \quad (2)$$

To help summarise the results presented here and in Section 4 two regions are defined that are representative of the ablation and accumulation zones. The areal distribution of these regions is determined using T_a isotherms. The ablation region is defined as the region where the summer mean $T_a > 3$ °C, which covers 10.2% of the total model ice sheet area of 1.76×10^6 km^2 and includes 66.0% of the simulated melt. The accumulation region is defined where the summer mean $T_a < -3$ °C, covering 49.0% of the ice sheet. These regions correspond to heights of 1115 and 2270 m, respectively, at a latitude of 72°N. The four energy balance components of the Greenland ice sheet, averaged over the summer season for the ablation and accumulation regions, are summarised in Fig. 2.

In the accumulation region the NSW contributes 53 W m^{-2} to the SEB. As discussed in DEN1, the simulated incoming radiation fluxes tend to be overestimated by the model when compared to observations made at three AWS sites in this region, namely Humboldt, Tunu-N and Summit (Steffen et al., 1996).

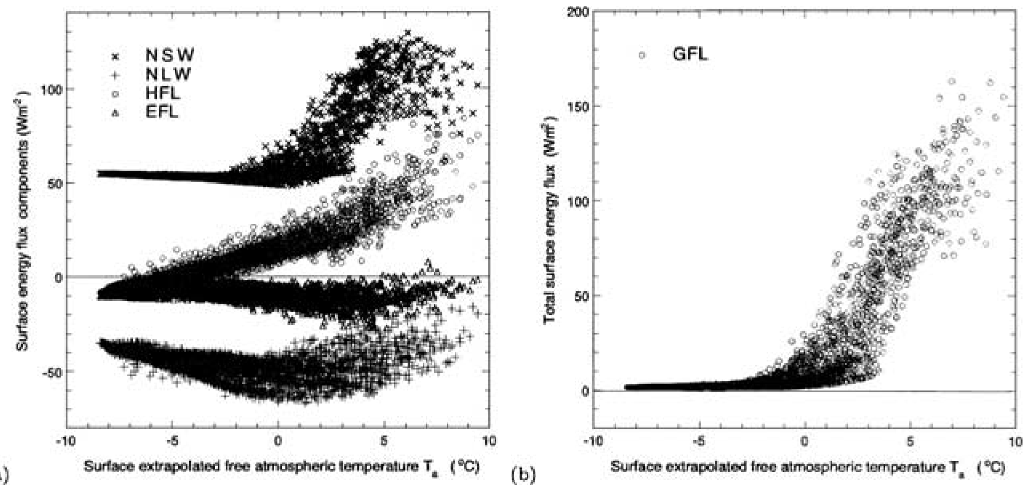

Fig. 1. (a) Mean surface energy balance components and (b) total surface energy flux as a function of the surface extrapolated free atmospheric temperature T_a. NSW is the net shortwave radiation, NLW the net longwave radiation, HFL the sensible heat flux, EFL the latent heat flux and GFL the total energy flux, all in W m^{-2}.

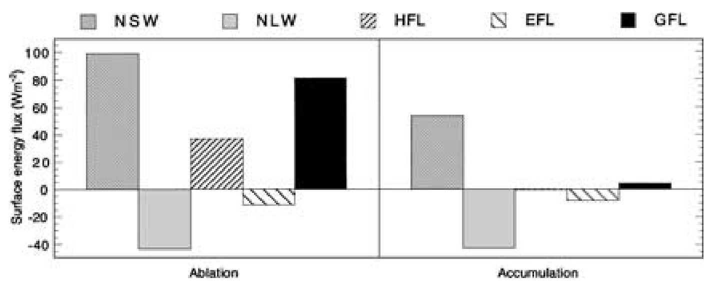

Fig. 2. Arealy averaged surface energy balance for the ablation and accumulation regions during the summer season. NSW is the net shortwave radiation, NLW the net longwave radiation, HFL the sensible heat flux, EFL the latent heat flux and GFL the total heat flux, all in W m^{-2}.

In the ablation region, where melting snow and ice surfaces lead to a lower albedo, NSW increases. Observations made at sites S5 and S6 indicate that these values are realistic.

In general NLW reflects the cloud cover distribution over most of the ice sheet. As the margin is approached, however, incoming longwave radiation will increase with increasing temperatures and the fixed surface melt temperature will keep the outgoing longwave radiation constant, leading to an increase in NLW towards the margin.

In the accumulation region the sensible and latent heat fluxes will tend to balance the radiation fluxes. Sensible and latent heat fluxes are both negative in the upper regions of the ice sheet, indicating a convective ABL which cools the surface. The presence of a convective ABL has been observed during summer by Box (2001) using AWS from the PARCA network. Because the SEB is almost balanced in this region the turbulent heat and outgoing longwave radiation fluxes, which are directly influenced by surface temperature, will adapt to the incoming radiation fluxes. Since the incoming radiation fluxes appear to be overestimated in the accumulation region it is likely that the turbulent heat fluxes will be in error in this region.

Near the ice margin both the sensible and latent heat fluxes can be seen to increase. The increase in sensible heat flux in the accumulation region is the direct result of the dominant downslope katabatic winds that advect stratified potentially warmer air down the sloping ice surface, increasing the temperature difference between ice and atmosphere. In regions where melt occurs the limiting surface temperature will enhance this difference. Latent heat flux is negative over almost all of the ice sheet but starts to increase near the margin. Katabatic winds will tend to advect dryer air downslope, leading to more evaporation and a lower latent heat flux. However, as the surface vapour pressure becomes limited by the melting point in the ablation region, evaporation from the surface will also decrease.

The total surface heat flux is small over the accumulation region, just 1.9 W m^{-2} on average. As surface temperatures increase with decreasing elevation, the limiting melting point temperature directly affects the SEB components. The excess energy is used to melt the surface in this region. This transition occurs at around $T_a = 0$ °C, where GFL can be seen to increase significantly (Fig. 1b).

In the defined ablation region, Fig. 2, the net radiation balance accounts for 68% of the total surface flux which is largely converted to melt. The turbulent heat fluxes account for the remaining 32%. This is a significant portion of the total melt, and indicates the importance of correctly simulating these fluxes in mass balance studies.

The average simulated melt over the entire ice sheet is 307 mm water equivalent (w.e.), which is roughly 85% of the climatological accumulation determined by Ohmura and Reeh (1991). The simulated melt must be considered an upper limit for the ablation since the model does not account for subsurface processes such as refreezing, so a large amount of the melt which occurs in snow covered areas will not contribute to the total ablation.

In a previous study of ablation on the Greenland ice sheet, van de Wal (1994) used a simplified energy balance model driven by the 2 m temperature parameterisation from Ohmura (1987). He found an average ablation of 189 mm w.e. with a parameterised description of refreezing in the snow and ice pack. Ohmura et al. (1996) also estimated the total ablation to be 200 mm w.e. based on the same temperature parameterisation and an observational relationship between temperature and ablation. However, it should be noted that the average 2 m temperature in the ablation region determined by GABLM for 1998 is roughly 1.2 °C higher than the temperature parameterisations used in those papers. Reeh (1991) also determined the mean ablation rate of the Greenland ice sheet to be 168 mm w.e. using a degree day model which incorporated refreezing in the snow pack and a similar temperature parameterisation.

4. Climate sensitivity

In this section a climate sensitivity experiment is carried out in order to determine the models sensitivity to an increase in free atmospheric temperature. The aim of this experiment is to quantify the sensitivity of the SEB as a result of an atmospheric temperature change. Particular attention is given to the turbulent heat fluxes as well as the 2 m meteorological variables that directly affect them. The sensitivity tests are carried out simply by increasing the ECMWF atmospheric temperature over the entire model domain by 1 K whilst keeping the relative humidity constant. The initial subsurface temperatures are also increased by the same amount. All other input parameters, such as cloud cover and sea surface temperature, are held constant. This method of testing the model sensitivity does not take into account changes in circulation that result from a global temperature change, but it does allow a less complicated investigation of the role temperature plays in determining the sensitivity of the SEB and near surface meteorological variables.

In the following discussion the climate sensitivity of some quantity, Φ, to a change in surface-extrapolated atmospheric temperature, T_a, is defined as

$$\mathrm{d}\Phi = \frac{\partial \Phi}{\partial T_a}. \tag{3}$$

This quantity is calculated from the model results by determining the difference between the sensitivity run and the reference run, resulting in a climate sensitivity per kelvin (K^{-1}).

Before discussing the climate sensitivity of 2 m meteorological variables and surface energy fluxes, it is informative to recap on the SEB as discussed in Section 3. The SEB components can be written in the following form:

$$\mathrm{NSW} = S_s(1-\alpha) \tag{4}$$

$$\mathrm{NLW} = L\downarrow_s - L\uparrow_s = \varepsilon_a \sigma T_a^4 - \sigma T_s^4 \tag{5}$$

$$\mathrm{HFL} = \rho_a c_p C_H U_{2m} \Delta T_{2m} \tag{6}$$

$$\mathrm{EFL} = \rho_a L_e C_E U_{2m} \Delta Q_{2m} \tag{7}$$

where the energy fluxes are described in terms of the surface-extrapolated free atmospheric temperature (T_a), the ABL temperature and specific humidity at 2 m (T_{2m} and Q_{2m}), and the surface temperature and humidity (T_s and Q_s). The difference between the 2 m and surface levels is written as ΔT_{2m} and ΔQ_{2m}. In the above equation $L\downarrow_s$ and $L\uparrow_s$ are the incoming and outgoing longwave radiation fluxes, ε_a is the effective emissivity of the atmosphere for the surface-extrapolated atmospheric temperature and the surface emissivity is assumed to be unity. The sensible (HFL) and latent (EFL) heat fluxes are described using the exchange coefficients C_H and C_E, which are related to surface roughness lengths, height and stability by

$$C_{H,E} = \kappa^2(P_r \ln(z/z_{h,q}) - \Psi_{h,q})^{-1}(\ln(z/z_o) - \Psi_m)^{-1} \tag{8}$$

in which z is the height above the surface, in this case 2 m, and the other terms are described in Eqs. (12) and (13) in DEN1. In these equations ρ_a is the density of air, c_p is the specific heat of air and L_e is the latent heat of vaporisation of water.

Differentiating the above equations with respect to a change in free atmospheric temperature T_a, assuming a constant relative humidity (R_{2m}), gives the following climate sensitivities for the surface energy flux components:

$$\mathrm{dNSW} = \mathrm{d}S_s(1-\alpha) - S_s\,\mathrm{d}\alpha \tag{9}$$

$$\mathrm{dNLW} = \mathrm{d}L\downarrow_s - \mathrm{d}L\uparrow_s = L\downarrow_s\left(\frac{4}{T_a} + \frac{\mathrm{d}\varepsilon_a}{\varepsilon_a}\right) - L\uparrow_s\frac{4}{T_s}\,\mathrm{d}T_s \tag{10}$$

$$\mathrm{dHFL} = \rho_a c_p\{(\mathrm{d}C_H)U_{2m}\Delta T_{2m} + C_H(\mathrm{d}U_{2m})\Delta T_{2m} + C_H U_{2m}(\mathrm{d}\Delta T_{2m})\} \tag{11}$$

$$\mathrm{dEFL} = \rho_a L_e\{(\mathrm{d}C_E)U_{2m}\Delta Q_{2m} + C_E(\mathrm{d}U_{2m})\Delta Q_{2m} + C_E U_{2m}(\mathrm{d}\Delta Q_{2m})\} \tag{12}$$

$$= \frac{L_e}{R_v T_s^2}\left(\mathrm{EFL}\,\mathrm{d}T_s + R_{2m}Q_s\frac{L_e}{c_p}\,\mathrm{dHFL}\right). \tag{13}$$

In the above equations use is made of the Clausius–Clapeyron equation in deriving Eq. (13) with the added assumption that $\Delta T_{2m} \ll T_{2m}$, where T_{2m} is in K.

4.1. Temperature sensitivity

In many energy balance and degree day models used to calculate ablation, climate sensitivity experiments are carried out by increasing a predefined near surface temperature field, usually at 2 m, by a fixed value. However, air temperatures in the ABL are affected by both surface and free atmospheric conditions and the change in 2 m temperature will not correspond directly to a change in free atmospheric temperature. The calculated average climate sensitivity of 2 m and surface temperature, $\mathrm{d}T_{2m}$ and $\mathrm{d}T_s$, for the summer season is shown in Fig. 3a as a function of T_a.

Let us firstly look at $\mathrm{d}T_{2m}$ in the non-melt areas of the ice sheet. Over most of the accumulation region $\mathrm{d}T_{2m} = 0.93$ except for Northern Greenland, where cloud cover is lowest, this can be greater than unity. The 2 m temperature sensitivity in non-melt areas is determined largely by the sensitivity of the longwave radiation flux. If a purely radiative change in energy balance is assumed, i.e. that changes in incoming longwave radiation are balanced by changes in outgoing radiation, then the surface temperature sensitivity will be given by $\mathrm{d}T_s = \varepsilon_a(T_s/T_{2m})^3$ if $\mathrm{d}\varepsilon_a = 0$. Typical values for ε_a in the non-melt region would then give $\mathrm{d}T_s = 0.80$. An increase in water vapour content will also lead to an increase in the effective emissivity which, using typical values derived from the model, would increase the surface temperature sensitivity by 0.15. In addition to these terms the latent heat flux, which has typical values of around -8 W m^{-2} in the accumulation region, will increase in magnitude with warming [Eq. (13)] leading to a slight decrease in the surface temperature sensitivity.

In regions where melt does take place, energy is transferred to the surface, and the surface temperature is limited for all or part of the ablation season by the melting point. Analysis of the SEB in this region will not give insight into temperature sensitivity, since this is the result of ABL dynamics, in which the balance between the turbulent diffusion and horizontal advection of heat are the dominant processes. The consequence of a fixed surface temperature is that 2 m temperatures will increase only fractionally as a result of a free atmospheric temperature increase. The transition seen in Fig. 3a from sensitivities close to unity in the accumulation region down to sensitivities of 0.3 in the ablation region is due mainly to the length of time the surface is limited by the melting point.

4.2. Wind sensitivity

In Fig. 3b the climate sensitivity of 2 m wind speed ($\mathrm{d}U_{2m}$) is shown as a function of T_a, where there is a general trend for increasing $\mathrm{d}U_{2m}$ with increasing T_a. As will be discussed, the driving mechanism for $\mathrm{d}U_{2m}$ is enhanced katabatic forcing, which is determined by surface slope and temperature inversion strength. Both these factors tend to increase with increasing T_a.

The dynamic structure of the ABL and its response to atmospheric warming can best be seen in the vertical profiles of wind and temperature and in the budget

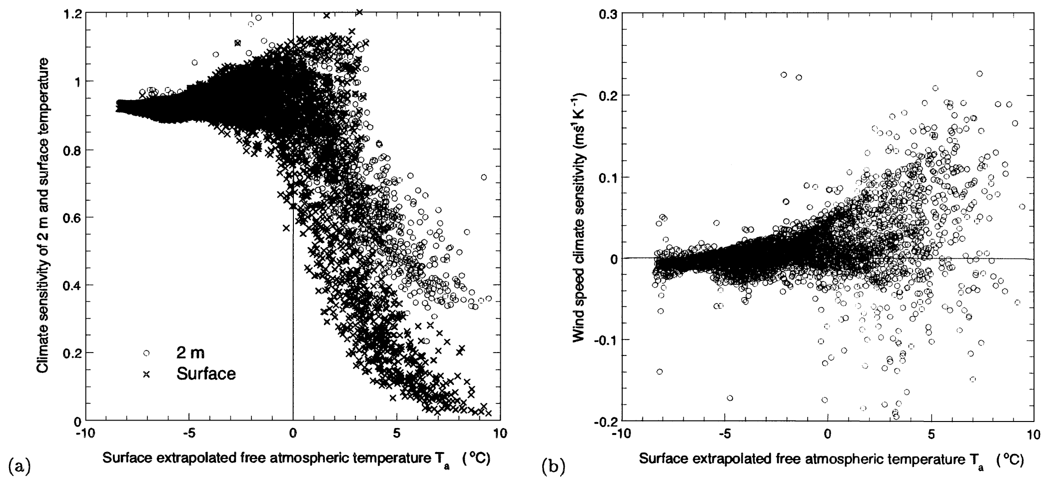

Fig. 3. (a) Climate sensitivity of 2 m and surface temperature as a function of T_a for the simulated summer period. (b) Climate sensitivity of 2 m wind speed as a function of T_a for the simulated summer period.

for momentum. In Figs. 4a–4c the summer average vertical profiles of wind speed, wind direction and temperature perturbation at site S6, which are typical of profiles along the Western margin, are shown. At this site a downslope flow corresponds to a negative U component. Clearly visible is the wind speed maximum at around 90 m, compared to the depth of the ABL of around 650 m. The wind turns from a South-Eastern direction of 134° near the surface to a Southern direction of 180°, perpendicular to the slope, at a height of 300 m. The downslope angle at site S6 is Eastern at 90°. Katabatic forcing in the lower part of the ABL drives the wind downslope, and Coriolis forcing turns the wind clockwise away from the downslope direction. The average geostrophic wind speed for this period is 5.3 m s^{-1} at 190°, which explains the large cross-slope component (V) in the upper ABL.

In Figs. 4d–4f the climate sensitivities of these variables are shown. When the climate sensitivity of temperature is less than unity, as in Fig. 4f, the temperature inversion strength will increase when free atmospheric temperature increases, with the resulting enhanced katabatic forcing. As expected wind speeds in the downslope direction U, Fig. 4d, are the most sensitive to enhanced katabatic forcing. Due to the large cross-slope component, V, the absolute change in wind speed, $\mathrm{d}|U|$, is less than the change in the downslope component $\mathrm{d}U$. The maximum wind speed sensitivity in the ABL at this site is 0.35 m s^{-1} K^{-1}, at around 40 m, whilst 2 m wind speed sensitivity is just 0.16 m s^{-1} K^{-1}. Similar results by van den Broeke (1997) have been found using a bulk model of the Greenland ABL with little synoptic forcing. He simulated a 6 m wind speed sensitivity near the margin of 0.3 m s^{-1} K^{-1}.

The momentum budget components in the ABL are shown, for the same site, in Fig. 5a. The momentum budget equation describing each component can be found in DEN1. In the lower part of the ABL, below 50 m, katabatic forcing (KAT) dominates and accelerates the wind in the downslope direction, which is retarded by the flux divergence (FLU) of horizontal momentum. Above 50 m both katabatic forcing and horizontal perturbation pressure gradient (PGR) are important terms. At this height, flux divergence becomes small and so the downslope acceleration is balanced almost completely by Coriolis forcing. Horizontal perturbation pressure gradients directed downslope will thus lead to cross-slope winds, as seen in Fig. 4a.

The climate sensitivity of the along-slope momentum budget at site S6 is also shown in Fig. 5b. Throughout the ABL the only major change in forcing with increased temperature comes from the katabatic term which is compensated for by the flux divergence of horizontal momentum.

4.3. Surface energy balance sensitivity

The climate sensitivity of the four SEB components averaged over the summer period are presented, as in Fig. 1, as a function of T_a in Fig. 6. These results are summarised for the ablation region in Fig. 7 along

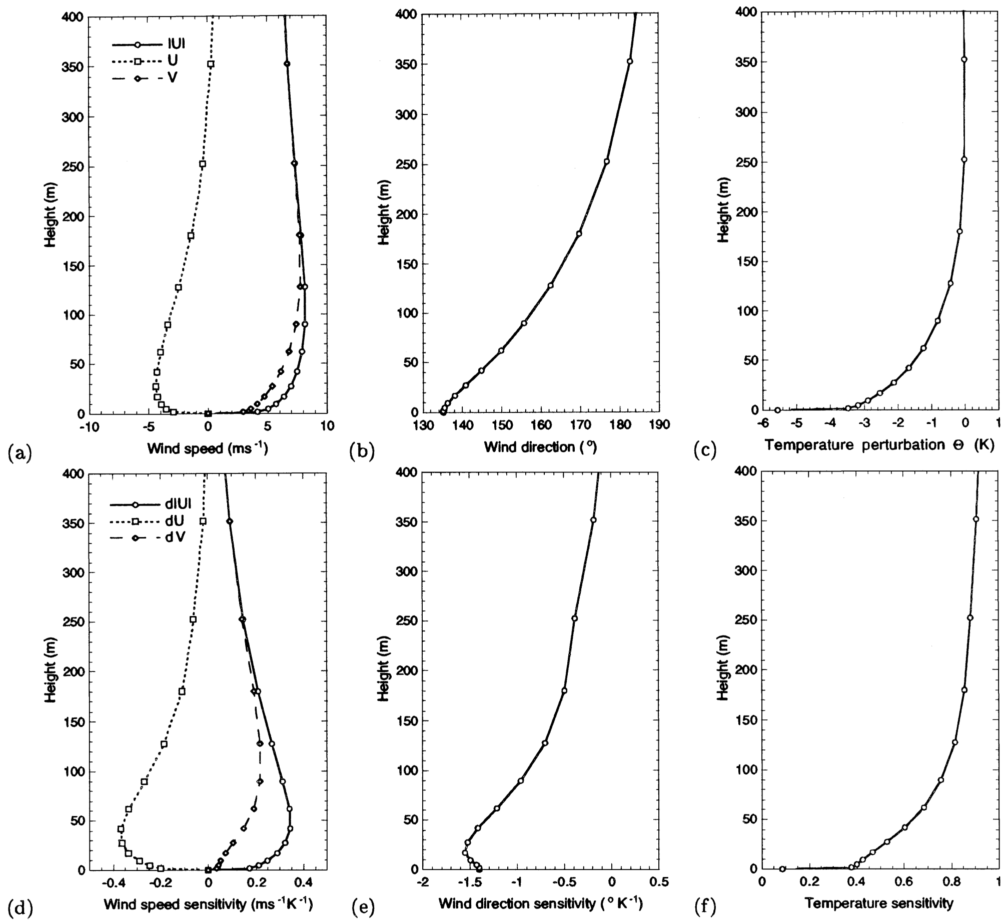

Fig. 4. Summer average vertical profiles of wind, wind direction and perturbation temperature at site S6 for the reference run. (a) Along-slope (U), cross-slope (V) and absolute ($|U|$) wind speeds where the downslope component U is negative. (b) Wind direction where the downslope direction is 90° at this site. (c) Temperature perturbation or temperature inversion strength Θ. (d)–(f) As in (a)–(c) but showing the climate sensitivity of these variables.

with the individual climate sensitivities for the three ablation sites S5, S6 and Swiss Camp. See DEN1 for a description of these three sites.

4.3.1. Radiation flux sensitivity. In the ablation region NSW radiation is the largest single contributor to the increase in surface energy flux. This is due to the albedo feedback mechanism [second term in Eq. (9)]. The increased melt that results from an increase in the turbulent heat and longwave radiation fluxes reduces the snow albedo and leads to enhanced melting through shortwave radiation absorption. In the model, incoming shortwave radiation attenuation is parameterised in terms of cloud cover and height, see DEN1. Since cloud cover is kept constant in the climate sensitivity run, incoming shortwave radiation will not be affected and $dS_s = 0$ [Eq. (9)].

In regions where the surface is bare ice for most of the melt season, e.g. close to the margin at site S5, the albedo feedback mechanism will not play an important role. The albedo feedback mechanism has thus a maximum effect in the region nearer to the snow line, e.g. S6 and Swiss Camp, where melt is generally low to begin with. The strength of the feedback will depend on the albedo parameterisation used. The form used here, see Eq. (28) in DEN1, allows snow albedo to decrease exponentially as a function of melt using a characteristic melt scale M^* and a limiting firn albedo. The value of M^* is not well defined and adjusting this

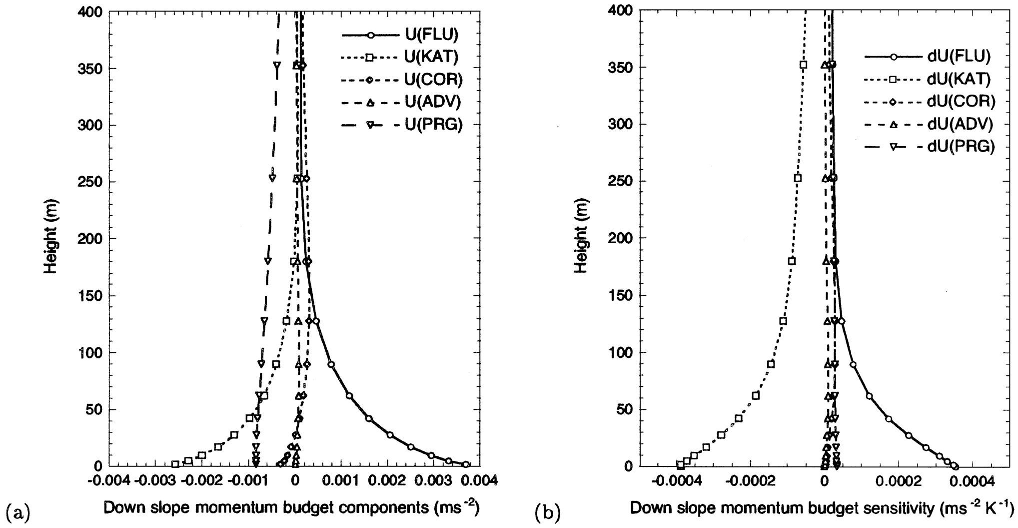

Fig. 5. (a) Summer average vertical profiles of the along-slope component of the momentum budget at site S6 in m s^{-1} K^{-1}. KAT is the katabatic forcing, COR the Coriolis forcing, ADV advection, PGR the horizontal perturbation pressure gradient and FLU the turbulent flux divergence of horizontal momentum. (b) As in (a) but showing the climate sensitivity of these components in m s^{-2} K^{-1}.

factor will alter the strength of the simulated albedo feedback. As such, some caution should be aired when attaching a quantitative value to the increase in surface energy flux as a result of albedo feedback, but the results from this study show that it can strongly enhance, by a factor of 1.7, the effect of the other energy flux components. This agrees with results from van de Wal (1996), for the Greenland ice sheet, and from Greuell and Böhm (1998), for an Alpine glacier, who found that the albedo feedback could double the total simulated melt, with a maximum just below the equilibrium line.

The climate sensitivity of the net longwave radiation flux, dNLW, is small in the accumulation region due to the response of the surface temperature to the changed forcing. In the ablation region, where $L\uparrow_{\mathrm{s}}$ remains fixed due to the limiting surface melt temperature, dNLW is greatest. In this region dNLW reflects the climate sensitivity of $L\downarrow_{\mathrm{s}}$, which results from the increase in atmospheric temperature and water vapour content. The climate sensitivity of the incoming longwave radiation flux, $\mathrm{d}L\downarrow_{\mathrm{s}}$, is given by Eq. (10) and is dependent on $L\downarrow_{\mathrm{s}}$, T_{a} and on the sensitivity of the effective emissivity, $\mathrm{d}\varepsilon_{\mathrm{a}}$, which is determined by the change in water vapour content, by the cloud cover and height, and by any variation in the ABL temperature profile as a result of a temperature change. One of the most important factors affecting $\mathrm{d}\varepsilon_{\mathrm{a}}$ is the cloud cover. With a totally overcast sky, the emitted longwave radiation from clouds can be approximated by a black body with a temperature equal to the cloud temperature. Because of this $\mathrm{d}\varepsilon_{\mathrm{a}}$ will be small when clouds are present. In Northern Greenland cloud cover is at a minimum of around 0.4, and it is in this region that $\mathrm{d}\varepsilon_{\mathrm{a}}$ and thus also $\mathrm{d}L\downarrow_{\mathrm{s}}$ are greatest.

The other factor that will affect $\mathrm{d}\varepsilon_{\mathrm{a}}$ is the alteration of the temperature profile. Because the climate sensitivity of ABL temperature in melt regions is less than unity (Fig. 4f), the effective emissivity will change as a result of the change in temperature profiles. This effect tends to reduce $\mathrm{d}\varepsilon_{\mathrm{a}}$. However, to a first approximation $\mathrm{d}L\downarrow_{\mathrm{s}}$ can be expressed in terms of Eq. (10), assuming $\mathrm{d}\varepsilon_{\mathrm{a}}$ to be zero. This results in an underestimation of $\mathrm{d}L\downarrow_{\mathrm{s}}$ by, on average, 1.0 W m^{-2} when compared with the simulated values.

4.3.2. Turbulent heat flux sensitivity. The climate sensitivity of sensible and latent heat flux as a function of T_{a} is shown in Figs. 6c and 6d, respectively. In non-melt regions the sum of these two components is close to zero, since the balance between incoming and outgoing longwave radiation accounts for most of the surface temperature increase. As the duration of surface melt increases with increasing temperature on

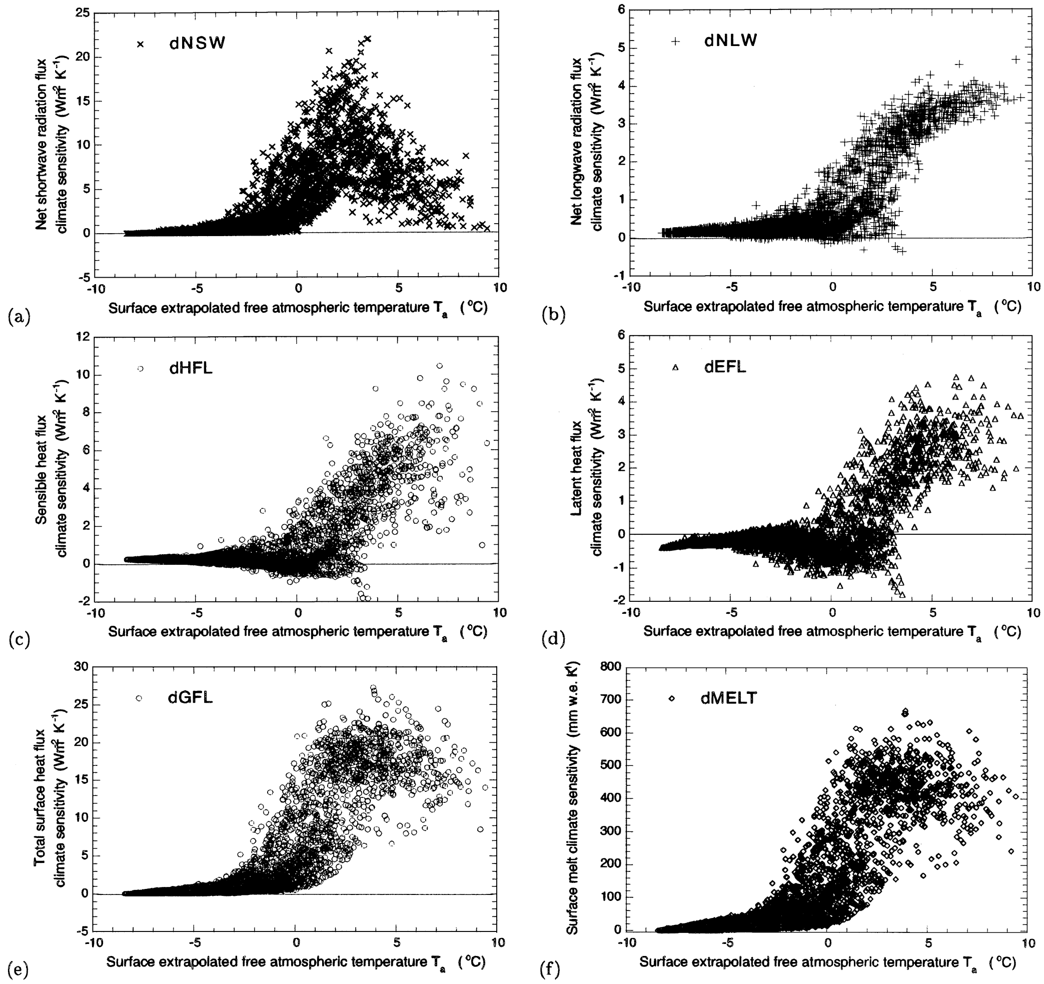

Fig. 6. Climate sensitivity of (a) the net shortwave radiation flux (dNSW), (b) the net longwave radiation flux (dNLW), (c) the sensible heat flux (dHFL), (d) the latent heat flux (dEFL), (e) the total surface heat flux (dGFL) and (f) the surface melt (dMELT). All are shown as a function of T_a for the simulated summer period.

the ice sheet the climate sensitivity of both turbulent flux components will be enhanced.

In the ablation region sensible heat flux is enhanced by an increase in both temperature and wind speed. However, the climate sensitivity of temperature is significantly larger than that for wind and will dominate dHFL. This increase is reflected in the climate sensitivity of the near surface temperature difference $d\Delta T_{2m}$ (Fig. 3a), which increases towards the margin as a result of increasing atmospheric temperature, of ABL dynamics and of the limiting surface melt temperature.

As discussed in Section 4.1, evaporation will be enhanced in the non-melt regions as a result of temperature increases. This is not the case in the ablation region due to the fixed surface temperature. When the climate sensitivity of the surface temperature, dT_s, is small or zero, i.e. melting, then dEFL will be directly proportional to the sensitivity of dHFL, if R_{2m} is unchanged, according to Eq. (13). dEFL is thus directly related to dHFL under these conditions by

$$\mathrm{dEFL} \cong \frac{R_{2m} Q_s L_e^2}{c_p R_v T_s^2} \mathrm{dHFL} \tag{14}$$

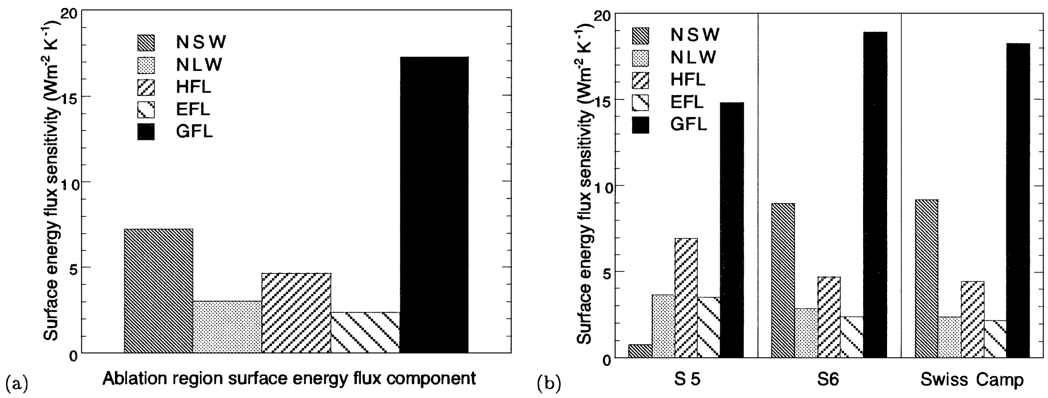

Fig. 7. Arealy averaged surface energy balance climate sensitivities for the predefined ablation region (a) and for the individual sites S5, S6 and Swiss Camp (b) during the summer season. Positions for these sites are listed in DEN1. NSW is the net shortwave radiation, NLW the net longwave radiation, HFL the sensible heat flux, EFL the latent heat flux and GFL the total heat flux. All climate sensitivities are given in W m^{-2} K^{-1}.

which means that the ratio dEFL/dHFL $\cong 0.7R_{2m}$ for conditions near the margin. Using a relative humidity of 80%, which is the average 2 m value calculated by the model in the ablation region, the relative sensitivity of dEFL and dHFL using Eq. (14) is very close to that determined by the model (Fig. 7a).

4.3.3. Components of the turbulent heat flux sensitivity. In Eqs. (11) and (12) the turbulent heat flux climate sensitivities are rewritten in terms of an exchange coefficient ($C_{H,E}$), 2 m wind speed (U_{2m}), and the difference between 2 m and surface values for temperature and water vapour (ΔT_{2m} and ΔQ_{2m}). Writing the equations for dHFL and dEFL in this form allows us to differentiate between the climate sensitivities of the various components involved. These are: changes in scalar roughness lengths $dC_{H,E}$, changes in wind speeds dU_{2m}, and changes in temperature and water vapour content $d\Delta T_{2m}$ and $d\Delta Q_{2m}$.

In Fig. 8 these three components are set out against the climate sensitivity of HFL and EFL as presented in Figs. 6c and 6d. The sensible heat flux climate sensitivity is clearly dominated by the change in temperature difference between the ABL and the surface. However, the enhanced wind speeds due to katabatic forcing, which are strongest near the margins, are responsible in some areas for up to 35% of the total climate sensitivity. As previously mentioned, geostrophic wind fields remain unchanged in the climate runs, so this will not affect the simulated wind speeds. The exchange coefficient is dependent on the surface roughness lengths for momentum, temperature and water vapour. Even though the surface roughness length for momentum is held fixed in all the simulations, the surface roughness length for temperature (z_h) can vary with wind speed. This is due to its dependence on the roughness Reynolds number, see Eq. (24) in DEN1, used to calculate z_h with surface renewal theories (Andreas, 1987). Increased wind speeds will lead to a decrease in the scalar surface roughness lengths according to this formulation.

For the latent heat flux, the dominant change is the result of an increase in specific humidity difference between the ABL and the surface, ΔQ_{2m}. The effects of wind speed and roughness lengths are small in comparison; however, enhanced wind speeds will tend to increase exchange with the surface and, since EFL is negative over almost all of the ice sheet, this will reduce the the climate sensitivity of EFL to a small extent.

4.3.4. Total surface energy flux sensitivity. The climate sensitivity of the total energy flux, dGFL, in the ablation region (Fig. 6e) is thus the sum of only positive effects, all components leading to an increase in GFL of 21% in the defined ablation region for a 1 K increase in atmospheric temperature. Because a significant increase in melt occurs outside the defined ablation region, due mostly to the albedo feedback mechanism, the total change in melt for the entire ice sheet is somewhat larger at 35%, see Fig. 6f. This is almost exactly the same value for the relative melt increase as arrived at by van de Wal (1994) using a simple parameterised form for the turbulent heat flux and longwave radiation.

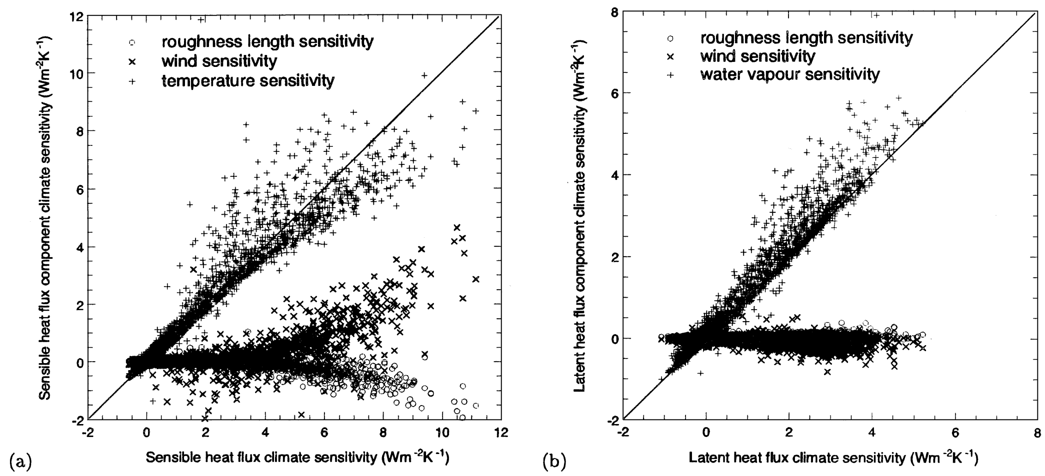

Fig. 8. The three components of the climate sensitivity for the sensible heat flux (a) and the latent heat flux (b) taken from Eqs. (11) and (12) and plotted against dHFL and dEFL. For dHFL these are roughness length sensitivity $[(\mathrm{d}C_{\mathrm{H}})U_{2\mathrm{m}}\Delta T_{2\mathrm{m}}]$, wind sensitivity $[C_{\mathrm{H}}(\mathrm{d}U_{2\mathrm{m}})\Delta T_{2\mathrm{m}}]$ and temperature sensitivity $[C_{\mathrm{H}}U_{2\mathrm{m}}(\mathrm{d}\Delta T_{2\mathrm{m}})]$ and for dEFL these are roughness length sensitivity $[(\mathrm{d}C_{\mathrm{E}})U_{2\mathrm{m}}\Delta Q_{2\mathrm{m}}]$, wind sensitivity $[C_{\mathrm{E}}(\mathrm{d}U_{2\mathrm{m}})\Delta Q_{2\mathrm{m}}]$ and water vapour sensitivity $[C_{\mathrm{E}}U_{2\mathrm{m}}(\mathrm{d}\Delta Q_{2\mathrm{m}})]$. The relationship between the exchange coefficients and surface roughness lengths is given in Eq. (8). All points on the ice sheet are used and the 1 : 1 line is also shown.

5. Summary and conclusion

Using an atmospheric boundary layer model, ECMWF analysis data is dynamically downscaled to a resolution of 20 km and the ABL of the Greenland ice sheet is simulated. The SEB of the ice sheet is determined and the various components of the SEB are discussed. In the defined ablation region, the radiation balance accounts for 68% of the SEB and turbulent heat fluxes for the remaining 32%. This reflects the importance of correctly simulating both these components if the SEB is to be well determined.

A climate sensitivity experiment is carried out to investigate the sensitivity of the SEB components and ABL properties such as temperature and wind. This experiment highlights a number of important points. Firstly, the climate sensitivity of 2 m temperature is less than unity in regions where melt occurs. This is the result of the limited surface temperature when ice and snow are melting. The mean sensitivity of the 2 m temperature is dependent on ABL dynamics and the duration of the surface melt. This is an important point when using mass and energy balance models that are driven by 2 m temperatures. A 1 K increase in 2 m temperature does not reflect the same increase in free atmospheric temperature but a significantly larger increase. Given a minimum climate sensitivity for 2 m temperature of 0.3, as determined in this study, then climate sensitivty experiments carried out with 2 m driven models would overestimate the climate senisitivity of the mass and energy balance by up to a factor of three.

Secondly, katabatic forcing will increase in the ablation zone as a result of an atmospheric temperature increase. The resulting enhanced wind speed contributes 12% to the total increase in sensible heat flux, when averaged over the entire ablation region. Since katabatic forcing is dependent on slope and inversion strength this will be most significant closest to the ice sheet margin where enhanced katabatic forcing contributes up to 35% to the sensible heat flux climate sensitivity.

Thirdly, the increase in the surface energy flux in the defined ablation region, as the result of a free atmospheric temperature increase of 1 K, is calculated to be 21% of the total surface heat flux. The three components of net longwave radiation, sensible heat flux and latent heat flux, which are directly affected by the temperature increase, make up 58% of the change in surface energy flux. The albedo feedback mechanism, whereby enhanced melt will lower albedo, can amplify these three components by a factor of 1.7.

The calculated average melt of 307 mm w.e. over the entire ice sheet is an upper limit for the total ablation since refreezing of melt water in the snow pack is not included in the model. The calculated climate sensitivity of melt over the entire ice sheet, calculated to be 109 mm w.e., will also represent an upper limit. However, the relative change in the total melt of 35% is very similar to that calculated by van de Wal (1994).

This study has highlighted some of the factors that influence the SEB and surface mass balance of the Greenland ice sheet. Katabatic winds have been shown to play a small but significant role in enhancing the sensible heat flux. The total contribution of the turbulent heat fluxes to the SEB has also been shown to be significant as has the role of albedo feedback in enhancing absorption of shortwave radiation. The boundary layer model used here has been specifically designed to investigate the role of turbulent fluxes in the SEB and as such has used simplifications for some of the other processes, e.g. shortwave radiation and subsurface processes. Clearly the logical step from here is to apply more complete mesoscale and subsurface models, at a similar resolution to this study, for longer periods in order to determine the current and possible future surface mass balance of the Greenland ice sheet.

6. Acknowledgements

This article has been significantly improved by the comprehensive critism of the reviewers and we wish to thank them for their time and effort. This research was chiefly funded by the Dutch National Research Programme on Global Air Pollution and Climate Change (NOP II project 013 001236.10).

REFERENCES

Andreas, E. L. 1987. A theory for the scalar roughness and the scalar transfer coefficients over snow and sea ice. *Boundary-Layer Meteorol* **38**, 159–184.

Box, J. E. 2001. *Surface water vapour exchanges on the Greenland ice sheet derived from automatic weather station data*. Ph.D. thesis, University of Colorado, USA.

Denby, B., Greuell, W. and Oerlemans, J. 2002. Simulating the Greenland atmospheric boundary layer. Part I: Model description and validation. *Tellus* **54 A**, this issue.

Ekholm, S. 1996. A full coverage, high-resolution, topographic model of Greenland computed from a variety of digital elevation data. *J. Geophys. Res.* **21**, 21961–21972.

Garratt, J. R. and Brost, R. A. 1982. Radiative cooling effects within and above the nocturnal boundary layer. *J. Atmos. Sci.* **38**, 2730–2746.

Glover, R. W. 1999. Influence of spatial resolution and treatment of orography on GCM estimates of the surface mass balance of the Greenland ice sheet. *J. Climatol* **12**, 551–563.

Greuell, W. and Böhm, R. 1998. 2 m temperatures along melting mid-latitude glaciers, and implications for the sensitivty of the mass balance to variations in temperature. *J. Glaciol.* **44**, 9–20.

Konzelmann, T., van de Wal, R. S. W., Greuell, W., Bintanja, R., Henneken, E. A. C. and Abe-Ouchi, A. 1994. Parameterization of global and longwave incoming radiation for the Greenland ice sheet. *Global Planet. Change* **9**, 143–164.

Ohmura, A. 1987. New temperature distribution maps for Greenland. *Z. Gletscherkd. Glazialgeol.* **23**, 1–45.

Ohmura, A. and Reeh, N. 1991. New precipitation and accumulation maps for Greenland. *J. Glaciol.* **37**, 140–148.

Ohmura, A., Wild, M. and Bengtsson, L. 1996. Present and future mass balance of the ice sheets simulated with GCM. *Ann. Glaciol* **23**, 187–193.

Reeh, N. 1991. Parameterization of melt rate and surface temperature on the Greenland ice sheet. *Polarforschung* **59**, 113–128.

Steffen, K., Box, J. E. and Abdalati, W. 1996. Greenland climate network: GC-Net. In: *CRREL 96-27 Special report on glaciers, ice sheets and volcanoes, trib. to M. Meier.* (ed. S. C. Colbeck) 101–123.

Thompson, S. L. and Pollard, D. 1997. Greenland and Antarctic mass balances for present and doubled atmospheric CO_2 from the GENESIS version-2 global climate model. *J. Climatol* **10**, 871–900.

van de Wal, R. S .W. 1994. An energy balance model for the Greenland ice sheet. *Global Planet. Change* **9**, 115–131.

van de Wal, R. S. W. 1996. Mass balance modelling of the Greenland ice sheet: a comparison of an energy-balance and degree-day model. *Ann. Glaciol* **23**, 36–45.

van den Broeke, M. R. 1997. A bulk model of the atmospheric boundary layer for inclusion in mass balance models of the Greenland ice sheet. *Z. Gletscherkd. Glazialgeol* **33**, 73–94.

Warwick, R. A., Provost, C. Le, Meier, M. F., Oerlemans, J. and Woodworth, P. L. 1996. *Changes in sea level.* In: *Climate change 1995* (ed. J. T. Houghton et al.). Cambridge University Press, Cambridge, UK, 359–405.

Zuo, Z. and Oerlemans, J. 1996. Modelling albedo and specific balance of the Greenland ice sheet: calculations for the Søndre Sstrømfjord transect *J. Glaciol.* **42**, 305–317.